ELSEVIER

Ceramics International 31 (2005) 461–468

CERAMICS INTERNATIONAL

www.elsevier.com/locate/ceramint

Comparison of the microstructures and ferroelectric characteristics of sputter deposited PZT films with and without lead or lead oxide for compensation

W.L. Chang*, J.L. He

Department of Materials Science, Feng-Chia University, No. 100, Wen-Hwa Road, Taichung, Taiwan

Received 22 January 2004; received in revised form 18 March 2004; accepted 10 June 2004
Available online 27 September 2004

Abstract

PZT thin films were deposited on $Si/SiO_2/Ti/Pt$ substrate using a dual-target system. A combination of a PZT ($PbZr_{0.54}Ti_{0.46}O_3$) single target, Pb/PZT ($PbZr_{0.54}Ti_{0.46}O_3$) dual targets and PbO/PZT ($PbZr_{0.54}Ti_{0.46}O_3$) dual targets, was used to reveal the effects of adding various lead source materials, on the microstructure and ferroelectric characteristics. Power delivery to the lead source and the deposition temperatures were investigated with respect to the microstructure and ferroelectric characteristics of the deposits.

The success in depositing perovskite PZT films using a Pb/PZT and PbO/PZT dual-target sputtering system presents the possibility of processing windows of substrate temperature between 500 °C and 580 °C. Structural change as a function of deposition conditions and lead sources correlated with ferroelectric characteristics.

Keywords: B. Microstructure; PZT thin film; Lead compensation; Ferroelectric characteristics

1. Introduction

Ferroelectric materials, such as lead-zirconate-titanate ($Pb(Zr_x,Ti_{1-x})O_3$, PZT) thin films exhibit high dielectric constants, high permittivity, pyroelectricity, ferroelectricity and piezoelectricity, as well as electro-optical and large spontaneous polarization characteristics. These characteristics enable PZT thin films to have application in a wide range of devices, including surface acoustic wave (SAW) devices, sensors, dynamic random access memories (DRAMs), non-volatile random-access memories (NVRAMs), accelerometers and transducers, among other devices [1–8].

PZT thin films have been prepared using various deposition techniques, such as metal organic chemical vapor deposition (MOCVD) [9] and sol–gel processing [10], which are chemical routes with metal organic precursors. Among the physical vapor deposition routes, laser ablation [11,12] allows stoichiometric deposition only with limited controllability and uniformity [13]. RF magnetron sputtering is associated with high crystallinity [14–17] and adjustable stoichiometry, governed by the plasma parameters; it is widely used in producing micro-electronic devices.

The composition of the film is one of the most important parameters in the preparation of PZT films, because the vapor pressure of Pb or Pb oxide is high enough that the Pb content of such films tends to be lead insufficient in high-temperature deposition. Attention has been paid to preparation by sputter deposition techniques, using various source (target) materials, such as the PZT ceramic target with excess Pb [18–21]; PbO/PZT dual targets [2,22,23]; the Pb–Zr–Ti three-metal target [24–26]; Pb pellets, and PbO pellets, have been fixed to variously designed Ti–Zr targets [27–29], as presented in Fig. 1a–c. Ti pellets and Zr pellets have been fixed to the Pb target, as shown in Fig. 1d; Pb, Zr and Ti metals have been combined attached to a single

* Corresponding author.

0272-8842/$30.00
doi:10.1016/j.ceramint.2004.06.011

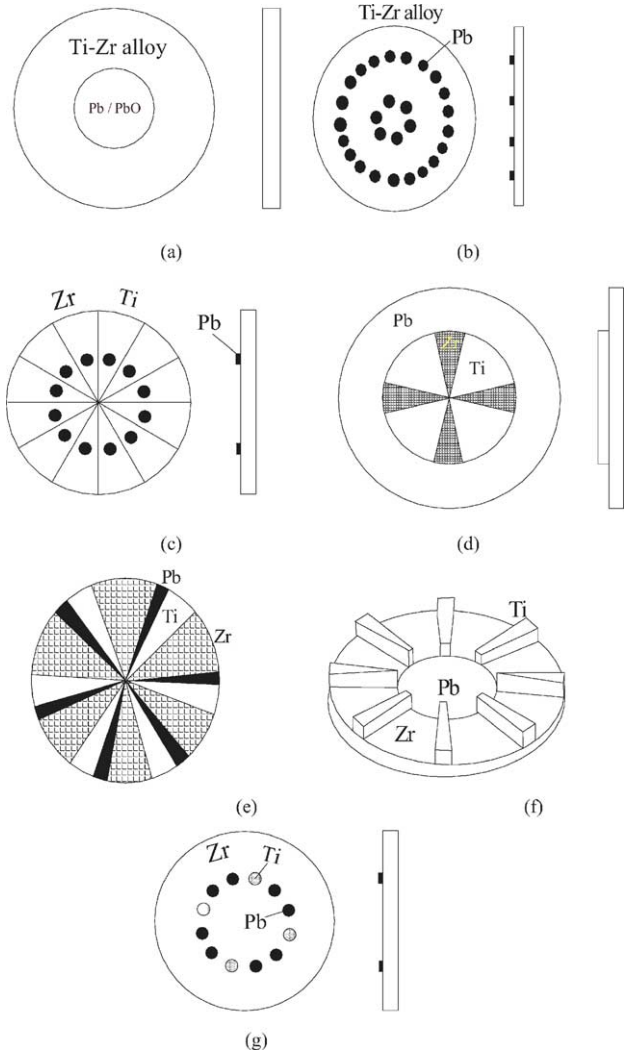

Fig. 1. Different target designs are used to deposit the PZT thin films.

target, as shown in Fig. 1e and f, and PbO pellets and Ti pellets have been fixed to a Zr target [30], as shown in Fig. 1g.

The thermal conductivity of ceramics is poor, so ceramic targets easily break during deposition at high target power and ensuring the stoichiometric composition of the PZT target during sintering is difficult because the vapor pressure is high. For a multi-element target, the poor control the composition of the film associated with sputtering yield differences among elements. Substitution of metallic Pb facilitates the fabrication of target material and the control of the Pb content of the film, while providing dc sputtering capability. Such a Pb/PZT combination has been rarely investigated.

This investigation deposits the PZT thin films on Si/SiO_2/Ti/Pt substrate using a dual-target system; a combination of a single PZT target, Pb/PZT dual targets and PbO/PZT dual targets was employed to reveal the effect of adding lead-compensating source materials on the microstructure and ferroelectric characteristics. Microstructure changes and ferroelectric characteristics are studied in relation to the deposition conditions.

2. Experimental

The substrates were Si(1 0 0) wafers with 150 nm-thick layers of thermally grown silicon dioxide, over which a 50 nm-thick titanium was deposited as an intermediate film and a 150 nm-thick platinum film was deposited as the bottom electrode. Deposition was performed using a double electron gun evaporator. The titanium film improves the adhesion of the platinum film and inhibits the diffusion of silicon into the platinum film, which would lead to the formation platinum silicides [31] and a loss of integrity of the platinum bottom electrode. The platinum film crystallized with a (1 1 1) texture.

Table 1 presents the deposition conditions of PZT films. Three target combinations were used, namely a PZT ($PbZr_{0.54}Ti_{0.46}O_3$) single target, Pb/PZT ($PbZr_{0.54}Ti_{0.46}O_3$) dual targets and PbO/PZT ($PbZr_{0.54}Ti_{0.46}O_3$) dual targets, respectively. In each coating run, the chamber was pumped down to an ultimate pressure of 1.2×10^{-3} Pa, and then argon gas was introduced to the coating chamber to increase the pressure to a working pressure of 0.15 Pa. The RF power of PZT target was maintained at 80 W, while those of the Pb target and the PbO target were varied from 15 W to 30 W and 15 W to 60 W, respectively. The substrate temperatures were varied from the ambient temperature to 580 °C, as measured by a well calibrated pyrometer. A film of uniform thickness

Table 1
Deposition conditions of the PZT films

Target combination	Single PZT target	Pb/PZT dual targets	PbO/PZT dual targets
RF power	PZT: 80 W	PZT: 80 W Pb: 15 W, 25 W, 30 W	PZT: 80 W PbO: 15 W, 30 W, 60 W
Target diameter	75 mm		
Sputtering gas	Ar		
Base pressure	1.2×10^{-3} Pa		
Working pressure	0.15 Pa		
Deposition time	2 h		
Substrate temperature	Ambient temperature to 580 °C		
Substrate material	$Pt/Ti/SiO_2/Si$		

PZT target composition: $PbZr_{0.54}Ti_{0.46}O_3$.

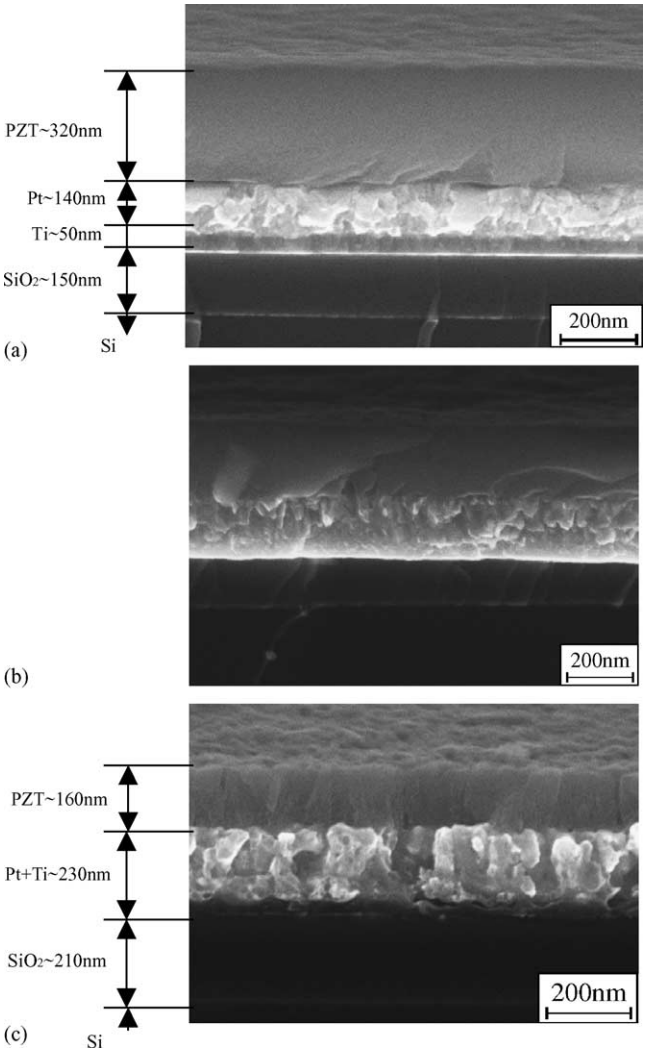

Fig. 2. Cross-sectional morphology of PZT films deposited by a single PZT target at (a) ambient temperature, (b) 400 °C and (c) 580 °C. PZT target power was 80 W.

and composition was obtained by rotating the substrate table during deposition.

The crystal structure of the deposited PZT films was identified using an X-ray diffractometer (XRD) with a Cu Kα source. The cross-sectional morphology of the deposited PZT films was observed by field emission scanning electron microscopy (FESEM). The compositional depth profile was determined by X-ray photoelectron spectroscopy (XPS). Ferroelectric polarization behavior was measured using a Radiant Technology RT66A tester. Before polarization was measured, a platinum layer with a diameter of 130 μm was deposited as the top electrode.

3. Results and discussion

Fig. 2 presents the cross-sectional morphology of PZT thin films deposited at various substrate temperatures using a single PZT target. Fig. 2a shows the smooth surface and featureless cross-sectional view of the film deposited at ambient temperature. The other parts of Fig. 2, in contrast, show films deposited at a higher temperature, which include columnar grains grown from the $Pt/Ti/SiO_2$ bottom electrode layer, whose thickness was increased by bottom layer/PZT or bottom layer/silicon substrate interdiffusion.

Figs. 3 and 4 show the cross sectional morphology of PZT films deposited using Pb/PZT and PbO/PZT dual targets combinations at various substrate temperatures, respectively. The dependence of the morphology on temperature is identical to that obtained using the PZT target, which is indicated in Fig. 2. One important difference between the micrographs obtained using three different target combinations is in the thickness of the film, and Fig. 5 presents growth rate as a function of substrate temperatures. The growth rate declined as the substrate temperature increased, regardless of the target combinations were used. This trend is a result of competition caused by the considerable difference between the activation energies of low-temperature phases and the high-temperature phases. The single PZT target, without added lead compensation, yields a relatively low growth rate over the entire range of substrate temperatures, as shown in Fig. 5a. When Pb/PZT and PbO/PZT dual targets combinations were used at Pb and PbO targets power deliveries of 15 W and 30 W, Pb/PZT yielded a higher growth rate than PbO/PZT because the sputter yield of Pb target exceeded that of the PbO target. Notably, the growth rate declined sharply with substrate temperature over 500 °C, indicating the

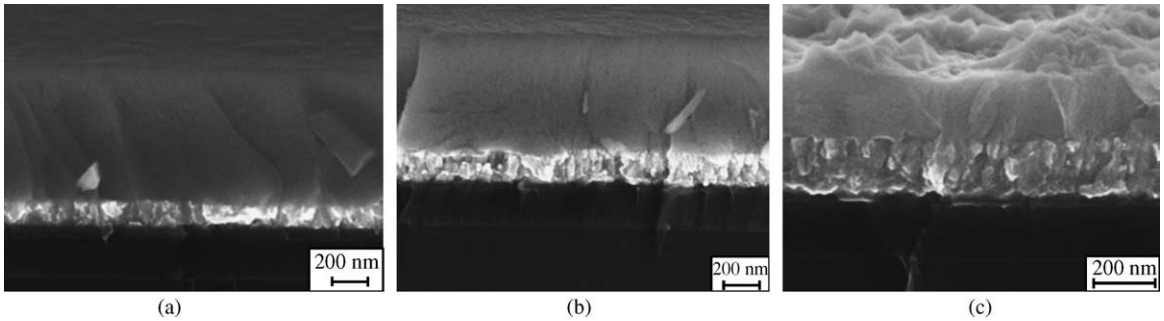

Fig. 3. Cross-sectional morphology of PZT films deposited at (a) ambient temperature, (b) 400 °C and (c) 580 °C using Pb/PZT dual targets. Pb target power was 25 W.

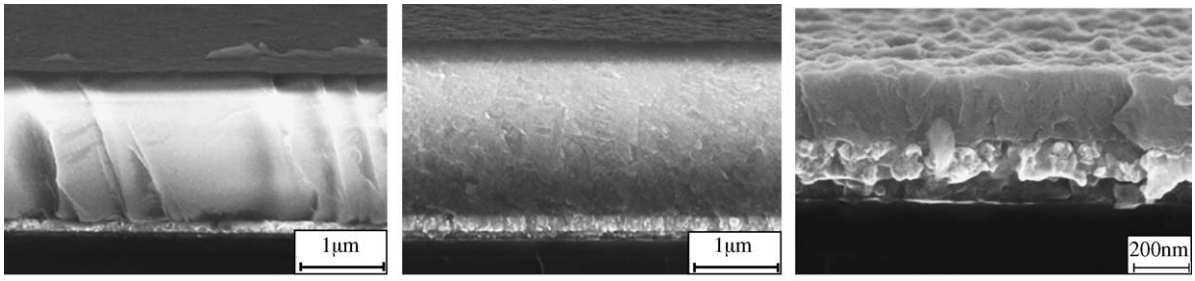

Fig. 4. Cross-sectional morphology of PZT films deposited at (a) ambient temperature, (b) 400 °C and (c) 580 °C using PbO/PZT dual targets. PbO target power was 60 W.

considerable change of the phase in the deposited films, as was further identified by XRD.

Fig. 6 presents the dependencies of XRD patterns of the PZT films prepared using a single PZT target on the substrate temperatures, given a target power of 80 W. The figure shows that the structures of the deposited PZT films have an amorphous phase that is independent of substrate temperature from ambient temperature to 580 °C. The XRD patterns in Fig. 7a show the structure of PZT films deposited at various substrate temperatures using Pb/PZT dual targets, with a Pb target power of 15 W. An amorphous phase is formed when is deposited at ambient temperature, and then the pyrochlore and PbO phases formed at 400 °C; the film includes only the pyrochlore phase at substrate temperatures of over 400 °C. Fig. 7b presents the amorphous phase of a PZT film deposited at ambient temperature with a Pb target power of 25 W. The PZT perovskite phase and the α-PbO_2 phase are both co-exist at 500 °C, and the films become predominantly perovskite phase at 580 °C. When the Pb target power is increased to 30 W, at under 400 °C, the phase does not differ notably from that obtained at a Pb target power of 25 W, as shown in Fig. 7c. The PZT film deposited at 500 °C reveals the coexistence of the pyrochlore phase and the α-PbO_2 phase; the films become predominantly perovskite at 580 °C.

The amorphous films formed at the substrate temperatures of below than 400 °C do not differ with the Pb target power, because the adatoms at the cold substrate surface insufficiently mobile to form a crystalline structure. Once the substrate temperature reaches the threshold temperature of 400 °C, it tends to form the pyrochlore phase because of its lower activation energy of formation than that of the perovskite phase, which requires a growth temperature of 580 °C. Adding an appropriate quantity of Pb to the deposited films, by controlling the Pb target power delivery to yield the desirable perovskite phase, is demonstrated herein.

The structures of the PZT films deposited using the PbO/PZT dual targets system at various substrate temperatures with a PbO target power of 15 W were identified by XRD,

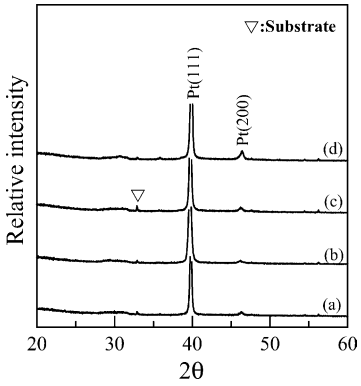

Fig. 6. XRD patterns of PZT films deposited using single PZT target at (a) ambient temperature, (b) 400 °C, (c) 500 °C and (d) 580 °C.

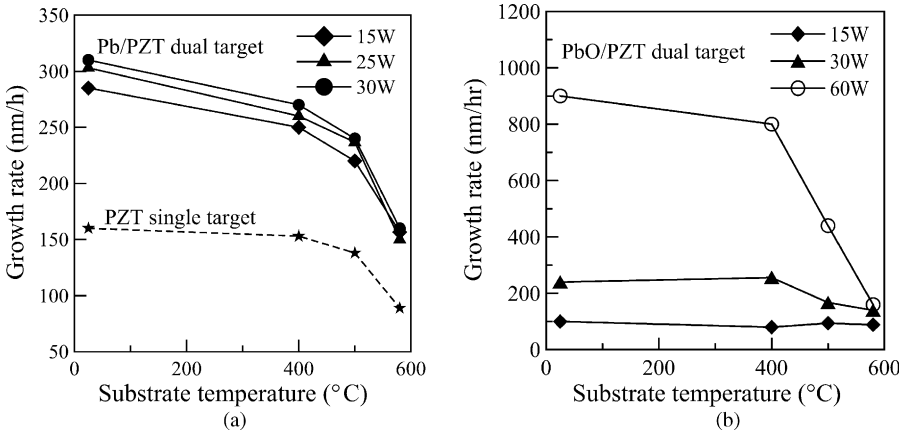

Fig. 5. Growth rate of PZT films as a function of substrate temperature, using (a) single PZT target and Pb/PZT dual targets, and (b) PbO/PZT dual targets.

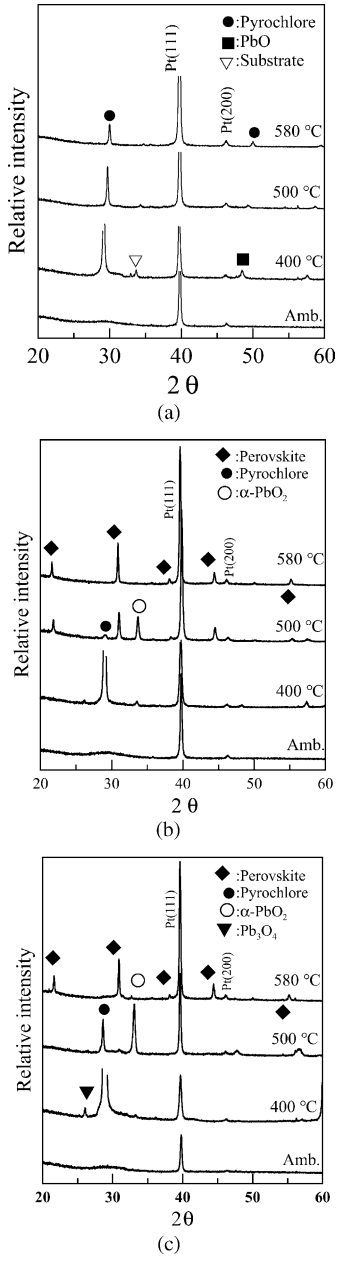

Fig. 7. XRD patterns of PZT films at various substrate temperatures and deposited using Pb/PZT dual targets with Pb target powers of (a) 15 W, (b) 25 W and (c) 30 W.

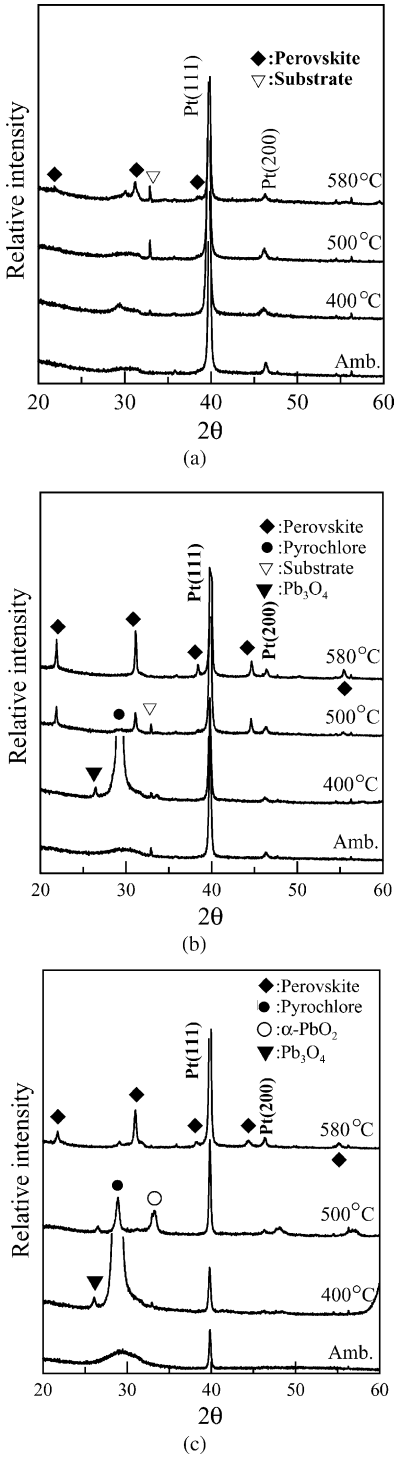

Fig. 8. XRD patterns of PZT films obtained at various substrate temperatures and deposited using PbO/PZT dual targets with PbO target powers of (a) 15 W, (b) 30 W and (c) 60 W.

the results of which are shown in Fig. 8a. Amorphous phases formed at temperatures from the ambient temperature to 500 °C, and the perovskite phase formed at 580 °C. The peak intensity of the substrate increased with the substrate temperature, indicating the very low growth rate, as already shown in Fig. 5b. Fig. 8b presents the structure of PZT films deposited using PbO/PZT dual targets with a PbO target power of 30 W at various substrate temperatures. The pryochlore phase was found to coexist with the Pb_3O_4 phase at 400 °C, but the films become predominantly perovskite phase at over 500 °C, indicating that the processing temperatures of the two target combinations extended to a relatively low value. Notably, optimizing the PbO target power delivery minimizes the substrate temperature required to form predominant perovskite phase. This temperature is lower than that requires in the sol–gel [32], MOCVD [33] and other sputtering processes [18,34]. As the PbO target power was increased to 60 W, the

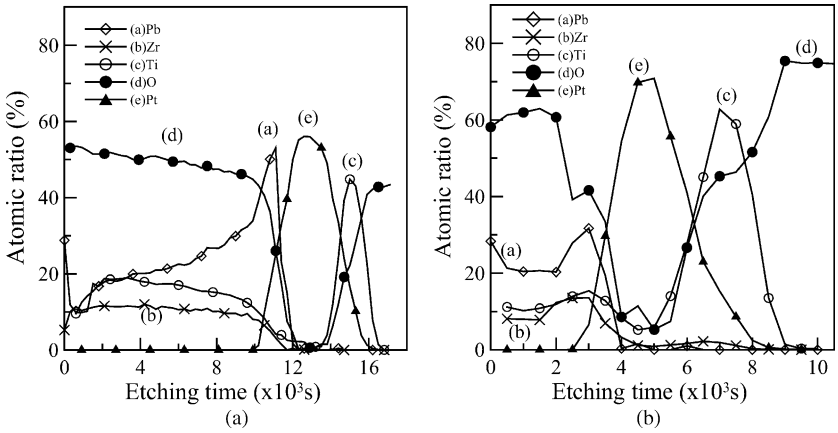

Fig. 9. Composition depth profiles of PZT films deposited using Pb/PZT dual targets at (a) ambient temperature, and (b) 580 °C. Pb target power was 25 W.

amorphous phase formed at ambient temperature, followed by pyrochlore and Pb_3O_4 phases at 400 °C, pyrochlore and α-PbO_2 phases at 500 °C and predominant perovskite phase at 580 °C. Accordingly, Pb compensation must be carefully controlled to yield predominant provskite phase.

These results show that the perovskite phase cannot be deposited using a single PZT ($PbZr_{0.54}Ti_{0.46}O_3$) target over the range of substrate temperatures studied herein, but can be deposited using the Pb/PZT dual targets at 580 °C, increasing the Pb content in PZT films favors growth. Similarly, the PbO/PZT dual targets favor the deposition of PZT films with the lowest substrate temperature of predominant perovskite phase formation at 500 °C, if the PbO target power is properly tuned.

Compositional depth profiles were studied to realize more deposited films using various target combinations. Fig. 9 shows the compositional depth profiles of the PZT films deposited at ambient temperature and 580 °C using the Pb/PZT dual targets with a Pb target power of 25 W. When the PZT films were deposited at ambient temperature, excess Pb near their top surfaces and at the PZT/Pt interfaces, were observed, and are shown in Fig. 9a. The excess Pb near the top surfaces is formed by the segregation of Pb outward toward the surface of the PZT and its oxidation to lead oxide [35]. The poor sticking coefficient of Pb allows Pb easily to diffuse through channels created by defects while the thin film is being prepared [36]. The better matching of the PbO lattice (a = 0.3972 nm) to the bottom Pt (a = 0.3923 nm) layer favors the formation of PbO during the first PZT growth stage, and later the growth of PZT (a = 0.48 nm) on this layer [35,37]. Hence, excess Pb is observed at the PZT film/Pt interface. When the PZT film was deposited at 580 °C, the Pb adatoms could not easily stay because Pb is volatile and has a high diffusion rate, so a smaller pile-up of Pb is observed at the PZT film/Pt interface in Fig. 9b. Fig. 9b also shows a thickening of the Pt and Ti layers due to interdiffusion at high temperature. Also, the overall thickness of the PZT in Fig. 9b is less than that in Fig. 9a, verifying the accuracy of Fig. 3. When the PbO/PZT dual targets was used, the compositional depth profiles of PZT films deposited at ambient temperature and 580 °C were as shown in Fig. 10a and b, respectively; they include the same features in those profiles obtained using the Pb/PZT dual targets, shown in Fig. 9a and b, respectively, but with a slightly lower Pb content.

The most interesting finding is the ferroelectric polarizability of each deposited PZT film. The film deposited using a single PZT target without a perovskite phase is least polarized, as shown in Fig. 11a. When Pb is added using Pb/PZT dual targets, polarization is maximum at a Pb target

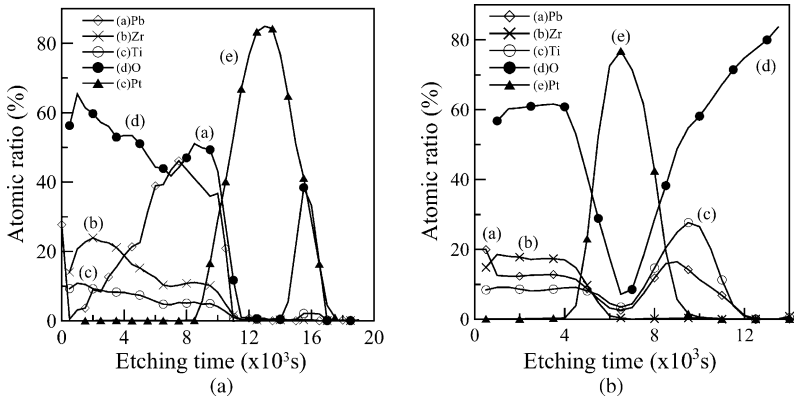

Fig. 10. Composition depth profiles of PZT films deposited using PbO/PZT targets at (a) ambient temperature, and (b) 580 °C. PbO target power was 60 W.

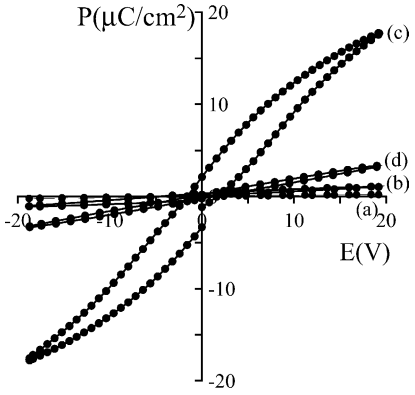

Fig. 11. Polarization behavior of the PZT films deposited by (a) single PZT target, and Pb/PZT dual targets with Pb target powers of (b)15 W, (c) 25 W and (d) 30 W. Substrate temperature was 580 °C.

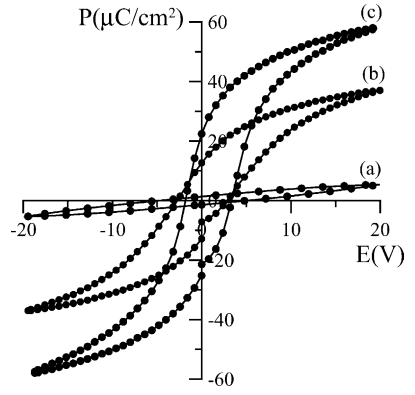

Fig. 12. Polarization behavior of the PZT films deposited by PbO/PZT dual targets with PbO target powers of (a) 15 W, (b) 30 W and (c) 60 W. Substrate temperature was 580 °C.

power of 25 W, as shown in Fig. 11c, indicating that an excessive target power of Pb at 30 W, over dosage of Pb could be easily generated due to the very high sputter yield. When PbO/PZT dual targets are used, polarization is maximum at a PbO target power of 60 W, indicating that polarization is not very sensitive to the low sputter yield of PbO, as shown in Fig. 12. In this study, the films deposited using PbO/PZT dual targets exhibit a higher saturation polarization than that deposited using Pb/PZT dual targets.

4. Conclusion

The successful deposition of perovskite PZT films on Si/SiO_2/Ti/Pt substrates can be achieved using Pb/PZT or PbO/PZT dual targets RF magnetron sputtering. Both means of Pb compensation can produce predominant provskite at a high substrate temperature although Pb/PZT exhibits a maximum polarization at a Pb target power of 25 W, indicating that a very high sputter yield can easily cause an excess Pb target power at 30 W. Maximum polarization can be obtained by PbO/PZT at a PbO target power of 60 W, indicating that polarization is not very sensitive to the low sputter yield of PbO. In this study, the films deposited using PbO/PZT dual targets exhibit a higher saturation polarization than that deposited using Pb/PZT dual targets.

Acknowledgements

The authors would like to thank the National Science Council of Taiwan, ROC, for financially supporting this research under Contract No. NSC 90-2745-P-035-004. Prof. K.C. Chen of the Department of Materials Science, Feng Chia University, is appreciated for his valuable discussions. M.Z. Lin's work in performing the coating runs and the help of Miss H.P. Wen at the Instrumentation Center of National Taiwan University in conducting XPS analysis are also greatly appreciated.

References

[1] R.N. Castellans, L.G. Feinstein, J. Appl. Phys. 50 (1979) 4111–4406.
[2] K. Abe, H. Tomita, H. Toyoda, M. Imai, Y. Yokote, Jpn. J. Appl. Phys. Pt. 1 30 (9B) (1991) 2152–2154.
[3] J.F. Scott, C.A.P.d. Araujo, Science 246 (1989) 1400.
[4] M. Sayer, K. Sreenivas, Science 247 (1990) 1056.
[5] T. Shiosak, IEEE (1990).
[6] B. Jaffe, W.R. Cook, H. Jaffe, Piezoelectric Ceramics, Academic Press, New York, 1971.
[7] P. Roychoudhary, S.B.D. Indian, J. Pure Appl. Phys. Rev. 22 (1984) 708.
[8] R. Lal, S.C. Sharma, R. Dayal, Ferroelectrics 100 (1989) 43.
[9] M. Cerqueira, R.S. Nasar, E.R. Leite, E. Longo, J.A. Varela, Ceram. Int. 26 (3) (2000) 231–236.
[10] R. Bruchhaus, Ferroelectrics 133 (1–4) (1992) 73–78.
[11] H. Kidoh, T. Ogawa, H. Yashima, A. Morimoto, T. Shimizu, Jpn. J. Appl. Phys. Pt. 1 31 (1992) 2965.
[12] S. Otsubo, T. Maeda, T. Minamikawa, Y. Tanezawa, A. Morimoto, T. Shimizu, Jpn. J. Appl. Phys. Pt. 1 29 (1990) L133.
[13] P. Verardi, F. Craciun, L. Mirenghi, M. Dinescu, V. Sandu, Appl. Surf. Sci. 138/139 (1999) 552–556.
[14] K. Iijima, I. Ueda, K. Kugimiya, Jpn. J. Appl. Phys. Pt. 1 30 (9B) (1991) 2149–2151.
[15] T. Hase, T. Shiosaki, Jpn. J. Appl. Phys. Pt. 1 30 (9B) (1991) 2159–2162.
[16] K. Sreenivas, M. Sayer, J. Appl. Phys. 64 (1988) 1484–1493.
[17] S.H. Oh, H.M. Jang, Appl. Phys. Lett. 72 (12) (1998) 1457–1459.
[18] T.S. Kim, D.J. Kim, J.K. Lee, H.J. Jung, J. Vac. Sci. Technol. A15 (6) (1997) 2831.
[19] Y. Park, K.W. Jeong, J.T. Song, Mater. Lett. 56 (4) (2002) 481–485.
[20] X.S. Li, T. Tanaka, Y. Suzuki, Vacuum 59 (2000) 800–805.
[21] F. Ayguavives, B. EA-KIM, B. Agius, Ferroelectrics 225 (1999) 229–236.
[22] T. Hase, T. Sakuma, Y. Miyasaka, K. Hirata, N. Hosokawa, Jpn. J. Appl. Phys. Pt. 1 32 (1993) 4061–4064.
[23] P. Padmini, R. Krawietz, R. Kohler, G. Gerlach, Ferroelectrics 228 (1–4) (1999) 79–89.
[24] R. Bruchhaus, H. Huber, D. Pitzer, W. Wersing, Ferroelectrics 127 (1–4) (1992) 137–142.
[25] H.J. Nam, D.K. Choi, W.J. Lee, Thin Solid Films 371 (2000) 264–271.

[26] K. Yamakawa, S. Trolier-McKinstry, J.P. Dougherty, Mater. Lett. 28 (1996) 317–322.
[27] T. Hata, S. Kawagoe, W. Zhang, K. Sasaki, Y. Yoshioka, Vacuum 51 (4) (1998) 665–671.
[28] W. Zhang, K. Sasaki, T. Hata, Jpn. J. Appl. Phys. Pt. 1 35 (9B) (1996) 5084–5088.
[29] W.X. Zhang, K. Sasaki, T. Hata, Jpn. J. Appl. Phys. Pt. 1 34 (9B) (1995) 5120–5123.
[30] W. Wang, T. Fujii, T. Karaki, M. Adachi, Jpn. J. Appl. Phys. Pt. 1 38 (1999) 6807–6811.
[31] D. Kaewchinda, T. Chairaungsri, M. Naksata, S.J. Milne, R. Brydson, J. Eur. Ceram. Soc. 20 (2000) 1277–1288.
[32] L.N. Chapin, S.A. Myers, Mater. Res. Soc. Symp. Proc. 243 (1992) 153.
[33] M.D. Keijser, D.J.M. Dormans, MRS Bull. 21 (1996) 37.
[34] C.K. Kwok, S.B. Desu, Ceram. Trans. 25 (1992) 85.
[35] A.R. Zomorrodian, A. Messarwi, N.J. Wu, Ceram. Int. 25 (2) (1999) 137–140.
[36] A.R. Zomorrodian, J. Sci. I.R. Iran 7 (4) (1996) 280.
[37] N.J. Wu, A. Ignatiev, A.W. Mesarwi, H. Lin, K. Xan, H.D. Shih, Mater. Chem. Phys. 32 (1993) 5019–5023.